Transformations of the distribution of nuclei formed in a nucleation pulse: Interface-limited growth

Vitaly A. Shneidman[a)]
Department of Physics, New Jersey Institute of Technology, Newark, New Jersey 07102, USA

(Received 18 June 2009; accepted 5 October 2009; published online 29 October 2009)

A typical nucleation-growth process is considered: a system is quenched into a supersaturated state with a small critical radius r_*^- and is allowed to nucleate during a finite time interval t^n, after which the supersaturation is abruptly reduced to a fixed value with a larger critical radius r_*^+. The size-distribution of nucleated particles $f(r,t)$ further evolves due to their deterministic growth and decay for r larger or smaller than r_*^+, respectively. A general analytic expressions for $f(r,t)$ is obtained, and it is shown that after a large growth time t this distribution approaches an asymptotic shape determined by two dimensionless parameters, λ related to t^n, and $\Lambda=r_*^+/r_*^-$. This shape is strongly asymmetric with an exponential and double-exponential cutoffs at small and large sizes, respectively, and with a broad near-flat top in case of a long pulse. Conversely, for a short pulse the distribution acquires a distinct maximum at $r=r^{\max}(t)$ and approaches a universal shape $\exp[\zeta-e^{\zeta}]$, with $\zeta \propto r-r^{\max}$, *independent* of the pulse duration. General asymptotic predictions are examined in terms of Zeldovich–Frenkel nucleation model where the entire transient behavior can be described in terms of the Lambert **W** function. Modifications for the Turnbull–Fisher model are also considered, and analytics is compared with exact numerics. Results are expected to have direct implementations in analysis of two-step annealing crystallization experiments, although other applications might be anticipated due to universality of the nucleation pulse technique. © *2009 American Institute of Physics*. [doi:10.1063/1.3254322]

I. INTRODUCTION

"Nucleation pulse," also known as two-step annealing in crystallization context[1–3] is a standard experimental technique to study intense nucleation in systems of diverse physical nature. During the first stage a system is quenched deeply into a metastable state, which is maintained during a "nucleation time" t^n, resulting in nucleation of a large number of particles in a relatively broad range of small sizes, typically of the order of nanometers or less. In exceptional situations ("single-step annealing" with long t^n) distribution of the largest particles can be observed directly,[4,5] but generally a second, growth stage of length t is required to bring particles to detectable sizes. Between the two stages the external control parameter, such as temperature[1–3] is abruptly changed, reducing the supersaturation and terminating nucleation. During the subsequent growth stage the change in sizes is enormous, up to three order of magnitude and more, and the challenge to a theoretical description is to extract the valuable, "microscopic" nucleation information from the observed distributions of large particles or, equivalently, to be able to predict those distributions once the nucleation part is assumed to be known.

In the past, the main focus of most of the related numerical[6–8] and analytical[9,10] studies was the total number of particles N, rather than the entire distribution $f(r,t)$. Partly, this was due to the relative simplicity of the associated mathematical problem when only the solution of the nucleation equation was required to find N. The growth stage then supplied a single parameter r_*^+, the corresponding critical size, to this solution without otherwise changing its structure—see Sec. II D below, while the values of the growth time had no effect. Partly, the exclusive interest in N was determined by the early crystallization experiments, where painstaking visual counting of hundreds of nuclei made it unrealistic to extract more detailed information about the distribution. However, advances in confocal microscopy combined with digital image processing[11] can provide more detailed information about the size distribution of microcrystals of the types observed in optical studies,[1,2] as well as in TEM,[3] which makes the theoretical evaluation of $f(r,t)$ a pertinent task.[12] Universality of the nucleation pulse technique allows to anticipate other applications, for example in vapor condensation where comparative numerical investigations of the pulse have been performed recently,[13,14] and where refined experimental data are available.[15]

The goal of the present paper is to describe analytically the time evolution of the distribution, with a special focus on the asymptotic behavior at large t. Although some general results, valid for any classical-type nucleation and growth will be presented, the major attention will be on the two mainstream models of interface-limited nucleation and growth. Those are the continuous Zeldovich–Frenkel (ZF)[16,17] and the discrete Turnbull–Fisher (TF) (Ref. 18) nucleation models. (Another discrete model, due to Becker and Döring[19,20] is expected to exhibit a qualitatively similar behavior, as described in the Appendix B.) The study expands

[a)]Electronic mail: vitaly@oak.njit.edu.

the one in a brief letter,[12] which also considers the diffusion-limited case.

Similarly to standard experimental assumptions, it is expected that interactions between nuclei are still negligible through the entire growth stage despite a significant increase in size. Those interaction can enter either via direct impingement of nuclei, as in the Kolmogorov–Avrami picture,[21,22] or, indirectly, via depletion of the matrix and continuous increase with time of r_*^+, as in the Lifshits–Slyozov–Wagner scenario.[23,24] This limits the total amount of the new phase, and thus the growth time t when the obtained solution can be used. Corresponding estimations are given in Sec. VI, and for the time scales considered restrictions on t are asymptotically weak provided the nucleation barriers are sufficiently large.

The present paper has the following structure. In Sec. II the system of notations is explained and the standard general relations between nucleation and growth are described, with an emphasis on the deterministic rate $\dot{r}$, which plays the central role in the forthcoming analysis. Specifications are made for the ZF model, and the transient nucleation distribution, which serves as initial condition for subsequent growth, is also presented.

In Sec. III evolution of the distribution $f(r,t)$ during growth is considered, with general results being conveniently expressed in terms of a "nascent size" $r_0(r,t)$, the size which will reach the observable size r after a growth time t. For $t \to \infty$ the nascent size becomes a function of a *single* parameter, indicating the emergence of an asymptotic shape.

In Sec. IV results are specified for the ZF model where $r_0(r,t)$ can be expressed explicitly through a special function. This allows a better understanding of the general asymptotic limits, but also clarifies the early time behavior when the growth and the decay regions start separating from each other with the most dramatic changes in the shape of the distribution. In particular, an interesting disappearance of the "nucleation singularity" at the smallest size is described.

In Sec. V modification of the asymptotic results for the TF model is discussed, and comparison with exact numerics for this model is presented. Section VI gives a qualitative description of the analytical results, as well as estimations of the domain of their applicability.

II. BACKGROUND

A. Notations for nucleation and growth stages

For clarity, parameters specifically related to the growth and the nucleation stages will be distinguished by superscripts + and − respectively; such superscripts, however, will be avoided in general definitions valid for both stages or when no confusion can occur, in expressions which are discussed exclusively for a single stage. The key functions which then determine the solution are $\dot{r}^{\pm}$, the deterministic growth rates for both stages, and the size-dependent flux j established by the end of the nucleation stage. Characteristic time scales $\tau^{\pm}$ are defined from corresponding growth rates, Eq. (7), and in specific examples the growth time t will be scaled by τ^+.

The dimensionless ratio of the critical radii

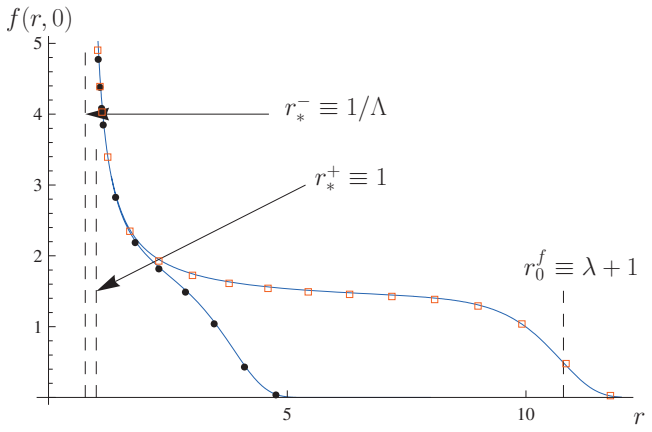

FIG. 1. Scaled distributions $f(r,0)/\tau^- j_{st}$ formed by the end of the nucleation pulse (initial conditions for growth), and explanation of notations. Lines—Eqs. (8) and (12) specified for the ZF model with $\Phi_*/kT \approx 37$ for two different durations of the pulse t^n, and with $\Lambda = 1.3$. Left curve: $t^n/\tau^- \simeq 10$, right curve: $t^n/\tau^- \simeq 20$; symbols—numerics. The small-r part is insensitive to t^n, which affects only the length of the tail (the initial location of the front, r_0^f, shown for the longer pulse). Particles with $r > r_*^+$ will grow to large sizes; the corresponding area under the curve, the scaled number of nuclei $N/\tau^- j_{st}$, is given by Eq. (10) and will be conserved upon further transformations. In the deterministic approximation the distribution has a singularity at $r = r_*^-$ which disappears after a short time t_d during the growth stage (Sec. IV A).

$$\Lambda \equiv r_*^+/r_*^- > 1,$$

will determine the relative depth of the nucleation quench, and for simplicity of notations the radii of nuclei r are assumed to to be scaled with r_*^+ (i.e., the latter can be taken as 1). The other dimensionless control parameter λ, related to the duration of the nucleation pulse t^n, corresponds to the length of the tail of the distribution at the end of the nucleation stage, as in Fig. 1. For a short pulse with t^n less than a few τ^-, when the nucleation distribution has no tail, an alternative to (possibly negative) λ will be used in the form of a dimensionless X, defined in Eq. (10) and related to λ either by the general Eq. (32) or by Eq. (19) for the mainstream nucleation model considered in specific examples.

The time t is counted from the instant when nucleation was terminated. When a discontinuity $t=0$ is important, the nucleation and the growth stages will be distinguished by $t = 0^-$ and $t = 0^+$, respectively.

B. Distribution and fluxes

Evolution of the distribution during growth is described by a continuity equation

$$\frac{\partial f}{\partial t} + \frac{\partial j}{\partial r} = 0, \tag{1}$$

with a drift approximation for the flux

$$j \simeq \dot{r} f. \tag{2}$$

Here $\dot{r}(r)$ is the deterministic growth rate, which depends on the mass exchange mechanism between the nucleus and the metastable phase or, in other words, depends on the specific nucleation model under consideration. A general feature is the change in sign of $\dot{r}(r)$ at the critical size r_*, reflecting the

decay of sub- and growth of supercritical particles, respectively.

In order to account for nucleation, a diffusive component should be added to the flux

$$j = -\beta\frac{\partial f}{\partial r} + \dot{r}f, \tag{3}$$

which makes Eq. (1) a Fokker–Planck type equation. According to Zeldovich[16] the "diffusion coefficient" in the r-space is related to deterministic rate by an analog of Einstein relation

$$\beta = -kT\frac{\dot{r}}{d\Phi/dr}, \tag{4}$$

where $\Phi(r)$ is the minimal work required to form a nucleus with a maximum $\Phi(r_*)\equiv\Phi_*$ corresponding to the nucleation barrier. In the standard ("classical") nucleation theory one has the Gibbs expressions

$$\Phi(r) = \Phi_*\left[3\left(\frac{r}{r_*}\right)^2 - 2\left(\frac{r}{r_*}\right)^3\right], \quad \Phi_* = \frac{4\pi}{3}\sigma r_*^2, \tag{5}$$

with σ being the interfacial tension.

Assuming an inhomogeneous boundary condition $f(r_{\min})=\text{const}\sim\exp[-\Phi(r_{\min})/kT]$ at some small $r_{\min}\ll r_*$, and an absorbing boundary in the growth region, one obtains the asymptotic expression for the steady-state flux in the limit $\Phi_*\gg kT$

$$j_{st} \sim \frac{1}{\tau}\exp\left(-\frac{\Phi_*}{kT}\right), \tag{6}$$

(which is remarkably insensitive to the precise location of those boundaries, provided they are far enough from r_*). The full pre-exponential was also evaluated in Ref. 16, although will not be required here as long as j_{st} is assumed to be *known*. The time scale τ, however, will be important. It is defined as[16]

$$\tau = \left(\left.\frac{d\dot{r}}{dr}\right|_{r=r_*}\right)^{-1}, \tag{7}$$

and should be specified, respectively, for the nucleation and for the growth stages. [On the other hand, the flux j_{st} with $\tau=\tau^-$ is evaluated only at the nucleation stage, and its value is assumed to be negligible for growth—see Sec. VI.]

C. Discrete nucleation models

An alternative to the Fokker–Planck type nucleation equation is the discrete, "Becker–Döring" (BD) equation,[20] written in the space of the number of monomers n in a nucleus—see Sec. V below. Selection of the discrete diffusivity β_n then specifies a model within the general scheme, with $\beta_n\propto n^{2/3}$ corresponding to the original BD choice, and an alternative being the TF selection, as described in Sec. V.

If τ follows the definition given by Eq. (7) and the nucleation barrier is large, the above asymptotic expression for j_{st} remains accurate, except possibly for very small values of the critical cluster number n_*.[25] However, the general connection between diffusivity and deterministic rate is different from Eq. (4) in the discrete case.[26,27] For the standard BD and TF models those rates are well known—see Appendix B and Sec. V, respectively.

Generally speaking, the time-dependent solutions of the discrete and continuous equations can differ significantly. In particular, at very small times $t\ll\tau$ a solution to the BD equation, which has no analog in the Fokker–Planck case, can be constructed.[28] This difference, however, is mostly of academic interest since at such small times the nucleation flux is virtually zero. For larger times $t\gtrsim\tau$ considered in the present work, modifications associated with switching between the discrete and continuous models are quite modest, and are solely due to the difference in the corresponding deterministic rates. Once corrections for those are introduced, the above Eqs. (1) and (2), as well as the general expressions for transient nucleation described below, can be used.

D. Transient nucleation and initial distribution for growth

Transient nucleation was described earlier[9,26] from the matched asymptotic (singular perturbation) solution of the BD equation in the same limit $\Phi_*\gg kT$. In present notations, the flux at the end of the nucleation stage is given by

$$j(r,0^-) = j_{st}\exp(-e^{-x}), \quad x\equiv[t^n - t_i(\Lambda r)]/\tau^-, \tag{8}$$

with the "incubation time" t_i at a given size $r>r_*^-$ related to the deterministic growth/decay rate $\dot{r}(r)$ by a general expression

$$t_i(r) = \mathbf{P}\int_0^r \frac{dr}{\dot{r}^-} + \tau^-\left(\ln\frac{6\Phi_*}{kT} - 2C\right),$$
$$C = \int_0^{r_*^-} dr\left(\frac{1}{\tau^-\dot{r}^-} - \frac{1}{r-r_*^-}\right). \tag{9}$$

Here $\mathbf{P}$ indicates the principal value of the integral and the constant C determines the nonlinear part of decay;[9] for the specific models considered explicit elementary expressions for $t_i(r)$ are available and will be discussed later in the paper.

Particles with size exceeding the new critical size r_*^+ will grow to large sizes and will be counted as "nucleated." Their number is given by the integral of Eq. (8);[9] in present notations

$$N(t^n) = \tau^- j_{st}E_1(e^{-X}), \quad X = \frac{t^n - t_i(\Lambda)}{\tau^-}, \tag{10}$$

where E_1 is the standard first exponential integral.[29] For $t^n\to\infty$ (large X) one has $E_1(e^{-X})\sim X-\gamma$, with $\gamma=0.5772\ldots$ being the Euler constant, and the dependence on nucleation time becomes linear

$$N(t^n) \simeq j_{st}(t^n - t_{\text{lag}}), \quad t_{\text{lag}} = t_i(\Lambda) + \gamma\tau^-. \tag{11}$$

In the above, t_{lag} is the time lag (also "induction time"), which is a direct experimental manifestation of transient nucleation.[1,2]

Once the flux is known, the distribution in the drift approximation is given by

$$f(r,0) = j(r,0^-)/\dot{r}^-. \tag{12}$$

The latter is valid for

$$r - r_*^- \gg \Delta_r \sim r_*^-(\Phi_*/kT)^{-1/2}, \tag{13}$$

with a small Δ_r indicating the width of the boundary layer near r_*^-.

A representative distribution for interface-limited growth is shown in Fig. 1. For a sufficiently long nucleation pulse the distribution acquires a tail of length λ, with a sharp cutoff ("front") at $r_0^f \equiv \lambda + 1$, defined as the root of an equation

$$t_i(\Lambda r_0^f) = t^n. \tag{14}$$

The parameter x in Eq. (8) is then given by

$$x = \int_r^{\lambda+1} dr/\tau^- \dot{r}^-. \tag{15}$$

For an exceptionally long pulse the tail approaches a constant $j_{st}/\dot{r}_\infty^-$, with $\dot{r}_\infty^- \equiv \lim_{r\to\infty} \dot{r}^-(r)$ being the growth rate in neglect of curvature effects.

E. Growth and transient nucleation in the Zeldovich–Frenkel model

The ZF model is usually associated with the continuous description given by Eqs. (1) and (3), with $\dot{r}$ specified for interface-limited growth at small supersaturations

$$\dot{r} = \frac{r_*}{\tau}(1 - r_*/r). \tag{16}$$

Together with Eqs. (4) and (5) this leads to diffusivity $\beta(r) = r_*^2\tau^{-1}(6\Phi_*/kT)^{-1}(r/r_*)^{-2}$ in the Fokker–Planck equation. Note that the dimensionless $\beta(r)/r_*^2$ is small for $r \sim r_*$, which determines the asymptotic accuracy of nucleation results described above. In addition, $\beta(r)/r_*^2$ becomes exceptionally small for a large $r \gg r_*$, leading to a negligible diffusion correction to the flux. Thus, if initial conditions for growth are accurately determined—see Fig. 1—one expects that further drift evolution, which is practically exact, will preserve the accuracy. (For which reason, further comparison with numerics for the ZF model will not be presented in this work; see, however, Ref. 12.)

With the adopted notations, the deterministic rate is specified for the growth and the nucleation stages

$$\dot{r}^+ = \frac{1}{\tau^+}\left(1 - \frac{1}{r}\right), \quad \dot{r}^- = \frac{1}{\Lambda\tau^-}\left(1 - \frac{1}{\Lambda r}\right). \tag{17}$$

The above relations will play a key role in the forthcoming discussion. The incubation time is given by[9]

$$\frac{1}{\tau^-} t_i(\Lambda r) = \ln\frac{6\Phi_*}{kT} - 2 + \Lambda r + \ln(\Lambda r - 1), \tag{18}$$

which gives

$$X = \frac{t^n}{\tau^-} - \ln\frac{6\Phi_*}{e^2 kT} - \Lambda - \ln(\Lambda - 1) = \Lambda\lambda + \ln\left(\frac{\Lambda\lambda}{\Lambda - 1} + 1\right), \tag{19}$$

and

$$x(r) = X + \Lambda(1 - r) + \ln\frac{\Lambda - 1}{\Lambda r - 1} \le X. \tag{20}$$

In the above it is assumed that the lower boundary of the Fokker–Planck equation is placed at a negligibly small size $r_{\min} \ll r_*^-$. If, for some reason this size is non-negligible, the incubation time must be reduced by the (positive) decay time from $r_{\min}$ to 0, which is $-\tau^-[\ln(1 - r_{\min}/r_*^-) + r_{\min}/r_*^-]$. When discussing the ZF model it is reasonable to avoid an extra parameter by ignoring the insignificant nonzero location of the boundary, typically placed at a few molecular sizes (while the critical size must be much larger in order to justify the model). It might be more important to account for $r_{\min}$ in discrete models (Sec. V) where the critical cluster number can be relatively small.

III. GENERAL

A. Arbitrary times

Since for any $t > 0$ the growth rate has no explicit time-dependence, the flux remains constant along the growth path, i.e.,

$$j(r,t) = j(r_0,0^+), \tag{21}$$

with the initial ("nascent") size $r_0(r,t)$ determined by the growth integral

$$\int_{r_0}^{r} \frac{dr}{\dot{r}^+} = t. \tag{22}$$

The distribution then can be determined from

$$f(r,t) = j(r_0,0^+)/\dot{r}^+. \tag{23}$$

On the other hand, the distribution (not the flux!) is continuous across $t = 0$, i.e., $f(r,0^+) = f(r,0^-)$. The latter can be related to nucleation flux by the drift approximation, Eq. (12), and this allows one to exclude the initial "growth" flux $j(r_0,0^+)$. One thus obtains

$$f(r,t) = j(r_0,0^-)\frac{\dot{r}_0^+}{\dot{r}_0^-\dot{r}^+}. \tag{24}$$

Together with Eq. (8) for the nucleation flux $j(r_0,0^-)$, the above result provides the full formal solution of the problem. In practice, one still needs to supply $r_0(r,t)$ from Eq. (22), which can be rather involved depending on the explicit expression for the growth rate for a selected model. At the moment, note that for any model $r_0(r,0) = r$, which gives the earlier $f(r,0) = j(r,0^-)/\dot{r}^-$.

Near the critical size $r_*^+ = 1$ the growth rate is approximated as $\dot{r}^+(r) \simeq (r-1)/\tau^+$, and Eq. (22) gives

$$r - 1 \simeq (r_0 - 1)\exp(t/\tau^+).$$

Thus, there is no singularity in the ratio $\dot{r}_0^+/\dot{r}^+$ in Eq. (24) and the distribution decreases exponentially with time

$$f(1,t) = \tau^- j_{st} \mu \exp(-e^{-X}) \exp(-t/\tau^+), \quad \mu \equiv \left. \frac{1}{\tau^- \dot{r}^-} \right|_{r=1}, \tag{25}$$

where X is related to nucleation parameters in Eq. (10). As a result, although the initial distribution is monotonic (Fig. 1), a maximum will be developed in the region of large sizes $r > 1$.

The general Eq. (24) is applicable both in the growth and the decay regions of sizes. Since the sign of $r_0 - 1$ is the same as of $r-1$, the ratio $\dot{r}_0^+/\dot{r}^+$ is always positive and so is the distribution. On the other hand, the solution is valid only for particles which were already growing during the nucleation stage, i.e., $\dot{r}_0^- > 0$ with $r_0 > 1/\Lambda$, with a singularity at the "old" critical size $1/\Lambda$. Restrictions on the physical size r, however, become weaker with time and after a *finite* decay time $t_d = -\int_0^{1/\Lambda} dr/\dot{r}^+$ the solution is applicable for any positive r. The singularity in the distribution drifts toward small sizes and disappears after the same decay time t_d. For larger t one expects $f(0,t) = 0$, as will be described later in the paper.

B. $t \to \infty$

After a sufficiently long growth time, the shape of a distribution is not expected to change anymore. To describe this effect, one needs to view this shape from a reference frame moving together with some representative particle, corresponding, say to the cutoff of the distribution or to its maximum.

Consider first a distribution with a well-developed initial front at r_0^f, as in Fig. 1. The position of the front $r^f(t)$ will evolve in accord with Eq. (22) with the lower and upper integration limits replaced, respectively, by r_0^f and $r^f(t)$. This allows one to eliminate time, and with the aforementioned notation $\lambda = r_0^f - 1$ one can write

$$\int_{r_0}^{\lambda+1} \frac{dr}{\dot{r}^+} + \int_{r^f(t)}^{r} \frac{dr}{\dot{r}^+} = 0. \tag{26}$$

The second integral can be simplified for $t \to \infty$ since typical r concentrate near $r^f(t)$. Introducing a dimensionless

$$\rho = \frac{r - r^f(t)}{\tau^+ \dot{r}_\infty^+(t)}, \tag{27}$$

with $\dot{r}_\infty^+$ being the growth rate of a large particle ("interface rate"), one thus has

$$\int_{r_0}^{\lambda+1} \frac{dr}{\dot{r}^+} \simeq -\rho\tau^+. \tag{28}$$

This is again an equation for r_0 but, unlike Eq. (22) which has both r and t as independent variables, in the present case r_0 is a function of a single variable ρ, indicating the emergence of an asymptotic shape.

Treating ρ as a new variable, and reducing the distribution by $\tau^- j_{st}$, one obtains the new dimensionless distribution in the ρ-space, $F(\rho) = F_0[r_0(\rho)]$ with

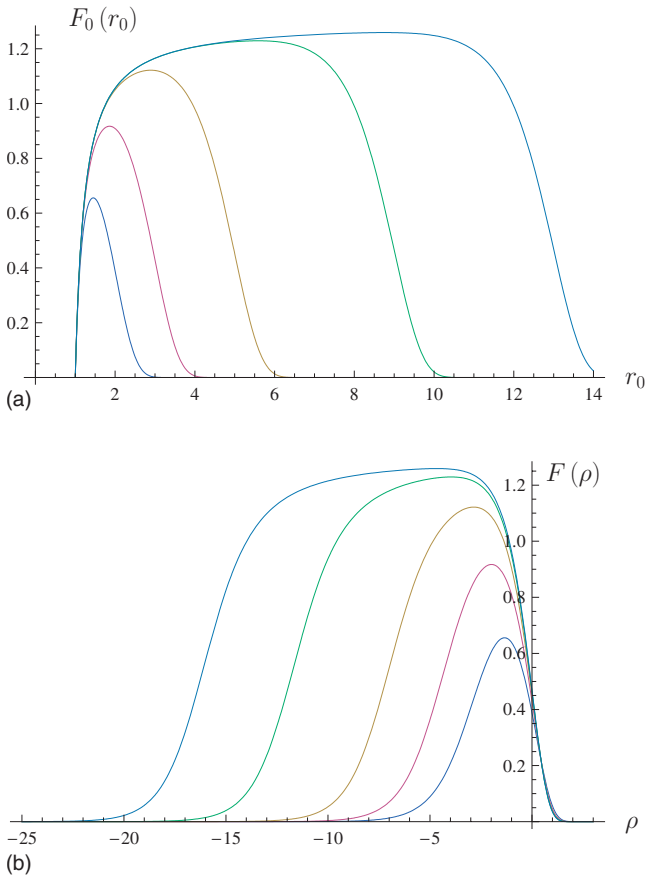

FIG. 2. Dimensionless asymptotic distribution in terms of (a) initial size r_0 and (b) in terms of $\rho = r - r^f(t)$, with $r^f(t)$ locating the front. For the ZF model the dependence $F_0(r_0)$ is elementary, Eqs. (20) and (54); $F(\rho)$ involves a special function, Eq. (56). For all curves $\Lambda = 1.3$ and, from left to right for (a) [from right to left for (b)], $\lambda = 1, 2, 4, 8, 12$; for selected nucleation barrier this would correspond to t^n/τ^- ranging, approximately, between 6 and 23—see Eq. (19).

$$F_0(r_0) = \frac{j(r_0, 0^-)}{j_{st}} \frac{\tau^+ \dot{r}_0^+}{\tau^- \dot{r}_0^-}. \tag{29}$$

The above two equations provide a parametric representation of the solution if r_0 is considered as an independent parameter. Often, the entire representation requires only elementary functions—see the ZF example later in the paper.

Unlike the general Eq. (24), the asymptotic distribution (29) is defined only for $r_0 \geq 1$. Smaller particles will decay and have no contribution at large time. The fact that ρ is the distance from the front did not play any special role so far, and a similar approach will be used in Sec. III E for distributions which are better characterized by a maximum.

A typical structure of the function $F_0(r_0)$ is shown in Fig. 2(a) for various durations of the nucleation pulse. Note that representation of the distribution as a function of ρ—Fig. 2(b)—requires a mere stretching of $F_0(r_0)$ in horizontal direction. Thus, that simpler function can be used, e.g., to evaluate the maximum. The actual structure of the distribution $F(\rho)$, however, will be better understood after the limits of a long and a short pulse are considered.

C. Moments of the distribution

Since a characteristic size associated with the distribution, say r^f, increases unboundedly during growth, one has

$$\frac{1}{\tau^- j_{st}} \int_0^\infty r^k f(r,t) dr = (r^f)^k M_0 + (r^f)^{k-1} k \cdot (\tau^+ \dot{r}_\infty^+)^1 M_1 + \cdots . \tag{30}$$

Here the dimensionless moments are defined in terms of ρ

$$M_k = \int_{-\infty}^{\infty} \rho^k F(\rho) d\rho = \int_{-\infty}^{X} \rho(x)^k \exp(-e^{-x}) dx, \tag{31}$$

The parameter X is given by

$$X = \int_1^{\lambda+1} \frac{dr}{\tau^- \dot{r}^-}, \tag{32}$$

and is equivalent to the one defined in Eq. (10). For $k=0$, Eq. (31) gives the earlier result for the number of nuclei N, the dimensionless part of Eq. (10), but otherwise the integral cannot be evaluated analytically. Certain simplifications are possible for a long pulse, as will be described below and in Sec. IV B.

D. Long pulse, $\lambda \gg 1$

In either variables r_0 or ρ—see, respectively, the curves with largest λ in Figs. 2(a) and 2(b), the distribution resembles an asymmetric trapezoid with a mild cutoff at small sizes, and a much sharper, "double-exponential" cutoff at large sizes due to transient effects at the beginning of nucleation.

Consider first the small-size cutoff with r_0 close to 1. Here the double-exponential factor, the dimensionless flux in Eq. (29), is close to 1, and taking the asymptote of the remaining part, one obtains

$$F_0(r_0) \simeq \mu(r_0 - 1), \tag{33}$$

with the constant μ defined in Eq. (25). The growth integral in Eq. (28) is now nearly divergent, implying $\rho \to -\infty$ and

$$r_0(\rho) \simeq 1 + \lambda e^{\rho + c(\lambda)}, \tag{34}$$

where

$$c(\lambda) = \int_1^{\lambda+1} dr \left(\frac{1}{\tau^+ \dot{r}^+} - \frac{1}{r-1} \right), \tag{35}$$

describes the nonlinear part of growth. Thus, in terms of ρ the small-size cutoff is *exponential* and is given by

$$F(\rho) \simeq \mu \lambda e^{\rho + c(\lambda)}. \tag{36}$$

The large-size cutoff takes place near the front $\rho \to 0$. Corresponding r_0 are close to initial $r_0^f = \lambda + 1$, or more accurately

$$r_0(\rho) \simeq 1 + \lambda + \rho \tau^+ \dot{r}^+ \big|_{r=\lambda+1}. \tag{37}$$

These values should be kept in the rapidly changing double-exponential, which determines the flux in Eq. (29). In the remaining part r_0 can be replaced by $\lambda+1$, leading to a simple shape of the front

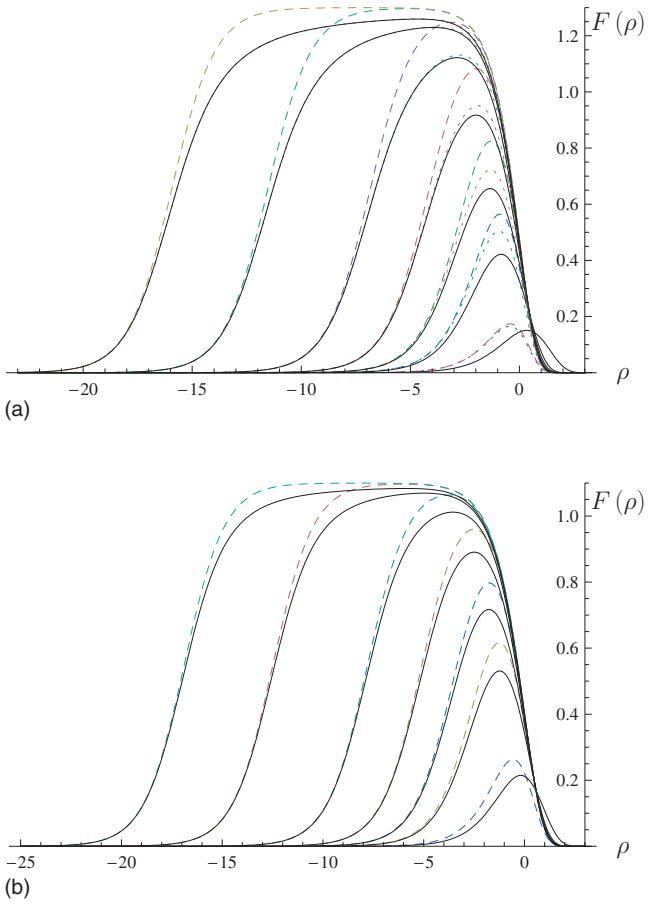

FIG. 3. Approximations to asymptotic distributions for not too short pulses for (a) $\Lambda = 1.3$ and (b) for $\Lambda = 1.1$. Solid lines are the full expression for different λ, as in Fig. 2, with added $\lambda = 0.1$ and $\lambda = 0.5$ (respectively, $t''/\tau^- \approx 4$ and 5). The small-Λ elementary approximation, Eq. (45), is shown by dashed lines. Dotted lines in (a) indicate the large-λ approximation, Eq. (60) (which blends in with the full expression for $\lambda \geq 8$).

$$F(\rho) \simeq \nu \exp(-e^{\nu\rho}), \quad \nu \equiv \left. \frac{\tau^+ \dot{r}^+}{\tau^- \dot{r}^-} \right|_{r=\lambda+1}. \tag{38}$$

A single interpolation which accounts for both cutoffs can be constructed, and will be discussed in connection with the ZF model—see Fig. 3. In between the cutoffs the distribution is near-flat and saturates at the same value ν, which becomes independent of the pulse duration if the latter is sufficiently long. For ultra long pulses, with λ in the range of hundreds,[12] both cutoffs become near-vertical and the distribution approaches a "box" shape.

For the purpose of evaluation of moments, note that the major contribution comes from large x with

$$\rho \simeq -x \frac{\tau^- \dot{r}_\infty^-}{\tau^+ \dot{r}_\infty^+},$$

and

$$\int_{-\infty}^{X} (-x)^k \exp(-e^{-x}) dx = (-1)^k \frac{X^{k+1}}{k!} + \mu_k + O(e^{-X}). \tag{39}$$

For reference, $\mu_0 = -\gamma$, $\mu_1 = \gamma^2/2 + \pi^2/12, \ldots$, etc. Similar numbers appear when evaluating temporal moments of the nucleation flux.[30] The odd-number moments M_k will be

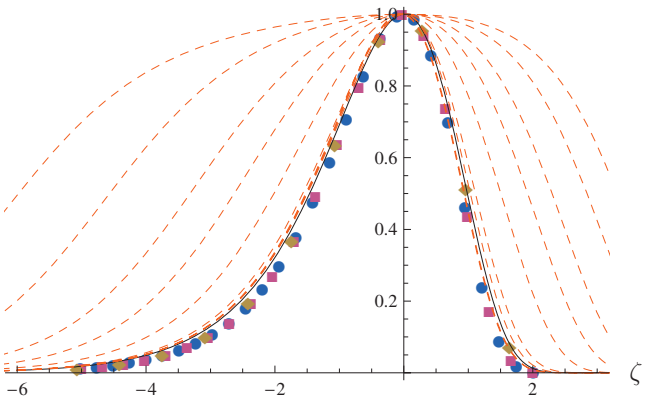

FIG. 4. Emergence of a universal shape, $\exp(1+\zeta-e^{\zeta})$ (solid line) in the limit of a short pulse. Dashed lines—analytical solutions of the ZF equation for different pulse durations. In order of decreasing width $t^n/\bar{\tau}=15, 12.5, 10, 4, 3, 2, 1, 0.5, 0.25$ (the last three curves practically blend with each other). Symbols—numerical solutions for the TF model at various pulse durations: $t^n=1.5$ (circles), 2 (diamonds), and 5 (squares), with the nucleation time scale $\bar{\tau}\approx 2$. Maxima of distributions are matched; other parameters including width, which emerges the same for short pulses, are not adjusted. In each case parameter ζ was defined as $(r-r^{\max})/\dot{r}_{\infty}$, with $\dot{r}_{\infty}$ being the growth rate of a large droplet. Absolute values of the maxima differ by orders of magnitude, and in units of $\bar{\tau} j_{st}$ are approximated by $9\cdot 10^{-7}$, 10^{-5}, and 2×10^{-2} for each of the TF pulses, respectively.

negative since the bulk of the distribution is at $\rho<0$.

E. Short pulse

Here for all sizes of interest the corresponding nascent size r_0 is close to 1. This gives

$$F_0(r_0)=\mu e^{-\alpha}(r_0-1)e^{-\alpha\mu(r_0-1)}, \tag{40}$$

with a constant

$$\alpha=e^{-X}\gtrsim 1. \tag{41}$$

Unlike the long-pulse situation, the distribution has a sharp maximum at $r_0^{\max}=1+1/\alpha\mu$ with a value

$$F^{\max}\approx e^{-\alpha-1}/\alpha,$$

which is extremely sensitive to the pulse duration. Once r_0 is expressed as a function of r and t, the maximum will be located at some $r^{\max}(t)$. A natural variable to describe the distribution will be the dimensionless distance from this maximum, ζ, defined quite similarly to ρ

$$\zeta=\int_{r_0^{\max}}^{r_0}\frac{dr}{\bar{\tau}^{+}\dot{r}^{+}}\simeq\frac{r-r^{\max}(t)}{\bar{\tau}^{+}\dot{r}_{\infty}^{+}}. \tag{42}$$

The corresponding distribution

$$F(\zeta)=\frac{e^{-\alpha}}{\alpha}\exp(\zeta-e^{\zeta}), \tag{43}$$

shown in Fig. 4 by a solid line. The shape is asymmetric with

$$\bar{\zeta}=-\gamma,\quad \overline{\zeta^2}=\gamma^2+\frac{\pi^2}{6}. \tag{44}$$

The most remarkable feature of this distribution is that its width is *independent* the pulse duration, as confirmed by numerical data (symbols) for the TF model described in Sec. V (and data for other models are discussed elsewhere[12]).

F. Shallow pulse, $\Lambda\to 1$

In this limit the shape of the distribution becomes especially simple. One has to show, however, that even for a small $\Lambda-1$ the increase in the nucleation barrier can be sufficient to terminate nucleation. Indeed, in the Gibbs expression for Φ_*, Eq. (5), the interfacial tension can be assumed a mild function of a control parameter, such as temperature. Thus, for a small increase in the critical size, the increase in the barrier is of the order of $2(\Lambda-1)\Phi_*$. Due a large value of Φ_* the increment of the barrier can still be much larger than kT, sufficient to terminate nucleation.

Using the connection between large negative ρ and r_0 in the ratio of growth rates in Eq. (29), and assuming not too small λ for a well-developed front, one obtains

$$F(\rho)\approx\frac{\Lambda\lambda}{\lambda+(1-1/\Lambda)\exp[-\rho-c(\lambda)]}\exp(-e^{\Lambda\rho}). \tag{45}$$

In practice, Λ exceeds 1 by about 30%. Nevertheless, the elementary approximation, which is valid for all ρ, can be useful for applications since it can provide reasonable accuracy even beyond its strict domain of validity, as in Fig. 3.

IV. APPLICATION TO ZELDOVICH–FRENKEL MODEL

With the simple growth rate of the ZF model, Eq. (17), the growth integral $\int dr/\dot{r}$ evaluates to a sum of a linear and a logarithmic terms and can be inverted in terms of the so-called Lambert **W** function. The latter function $\mathbf{W}[z]$ is defined as the root of an equation

$$z=\mathbf{W}e^{\mathbf{W}},$$

and can be used (a) to express explicitly $r_0(r,t)$, (b) to determine $r_0(\rho)$ in the asymptotic dependence, and (c) to relate the initial front position r_0^f, which is the root of Eq. (14), to nucleation parameters, specifically to the pulse duration t^n. Other expressions are also simplified since the incubation time $t_i(r)$ in Eq. (18) is an elementary function. To compress notations, the growth time t will be further scaled by $\bar{\tau}^{+}$.

A. Initial transformations of the distribution

With the above definition of the Lambert **W** function, the nascent size r_0 is given by

$$r_0(r,t)=1+\mathbf{W}[(r-1)e^{r-t-1}], \tag{46}$$

where $r_0(r,0)=r$ and $r_0(1,t)=1$, as expected.

The initial position of the front is determined by

$$r_0^f\equiv\lambda+1=\frac{1}{\Lambda}\{1+\mathbf{W}[e^{X+\Lambda-1}(\Lambda-1)]\}, \tag{47}$$

with X related to nucleation parameters by Eq. (19). The front further evolves with time in accord with

$$r^f(t)=1+\mathbf{W}[\lambda e^{\lambda+t}]. \tag{48}$$

Distribution at arbitrary time is given by Eqs. (8) and (24). The parameter x in Eq. (8) is now given by elementary Eq. (20) with r replaced by r_0, from Eq. (46). Explicitly, one has

$$f(r,t) = \Lambda^2 \bar{\tau} j_{st} \frac{r_0 - 1}{\Lambda r_0 - 1} \frac{r}{r-1} \exp\{-\exp[-x(r_0)]\},$$

$$r_0 = r_0(r,t). \tag{49}$$

Note that zero in the denominator at $r=1$ is fictitious and is cancelled with the one in the numerator in view of $r_0(1,t)=1$. On the other hand, the singularity at $r_0=1/\Lambda$ can be real, reflecting a rapid increase in the distribution toward the nucleation critical size $r_*^-=1/\Lambda$. Whether this singularity is observed or not, depends on whether the equation $r_0(r,t)=1/\Lambda$ has a solution with a positive r. The latter limits the time by t_d, the decay time for a particle with initial size $1/\Lambda$

$$t_d = \ln\frac{\Lambda}{\Lambda - 1} - \frac{1}{\Lambda}. \tag{50}$$

The most intriguing part is the disappearance of the singularity at $t=t_d$, as described below.

Consider a small size $r \ll 1$, and t close to t_d. In that case $\dot{r}^+ \simeq -1/r$ and

$$r_0(r,t) \simeq \frac{1}{\Lambda} + (\Lambda - 1)(r^2/2 + t - t_d). \tag{51}$$

The distribution at small r is thus approximated by

$$f(r,t) \simeq \bar{\tau} j_{st} \frac{r}{r^2/2 + t - t_d}. \tag{52}$$

Two distinct situations are possible. For $t<t_d$ the distribution is defined only for $r>\sqrt{2(t_d-t)}$, and is singular when r approaches the lower boundary. At $t=t_d$ the singularity abruptly disappears, indicating the dissolution of a large number of small nuclei which did not survive growth. For larger times $t>t_d$ the distribution is defined for all $r \geq 0$, and linearly tends to zero for $r \to 0$.

B. Transition to asymptotic shape

1. Arbitrary pulse

For the ZF model parameter ρ defined in Eq. (27) has a direct meaning of the distance from the front

$$\rho = r - r^f(t). \tag{53}$$

Viewed from a corresponding reference frame, as in Fig. 5, the distributions indeed quickly approach an asymptotic shape. The latter is given by

$$F_0(r_0) = \Lambda^2 \frac{r_0 - 1}{\Lambda r_0 - 1} \exp\{-\exp[-x(r_0)]\}, \tag{54}$$

with $x(r_0)$ defined in Eq. (20) but with r_0 being a function of a *single* parameter ρ, which follows from an equation

$$\rho = r_0 - 1 - \lambda + \ln\frac{r_0 - 1}{\lambda}. \tag{55}$$

The latter has a solution

$$r_0(\rho) = 1 + \mathbf{W}[\lambda e^{\rho+\lambda}], \tag{56}$$

with asymptotes $1+\lambda e^{\rho+\lambda}$ for $\rho \to -\infty$ and $1+\lambda+\rho\lambda/(1+\lambda)$ for $\rho \to 0$, respectively, in accord with Eq. (37). The asymptotic shape is a nontrivial function of two parameters, Λ and λ, and has a strict zero at the critical size, corresponding to $r_0=1$. There is no subcritical distribution anymore or singularities since $r_0 \leq 1$ cannot be achieved.

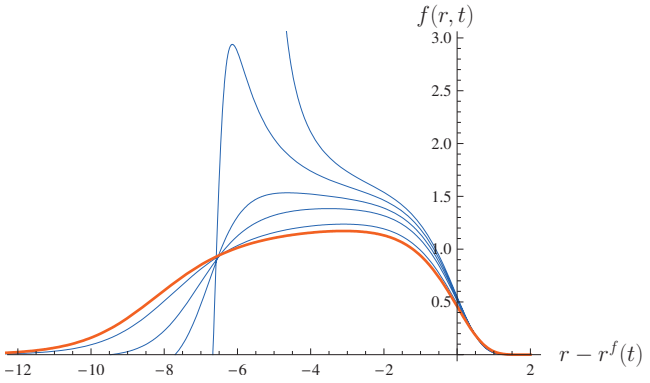

FIG. 5. Scaled distribution at various growth times t, as seen from a reference frame moving with the front. From top to bottom: $t=0,0.8,2,4,16$ (with $\Lambda=1.3$ and $\lambda=5$, or $t''/\bar{\tau} \approx 13$, for all curves). Thick solid line—asymptotic distribution $F(\rho)$.

Simplifications of the general asymptotic expression are possible if parameter X is large, implying a separation of the cutoffs. From Eq. (19) one concludes that X can be large either when Λ is close to 1 ("shallow pulse") and/or when λ is large ("long pulse"). The resulting approximations are discussed below.

2. Shallow pulse

For $\Lambda \to 1$ and not too small λ, the cutoffs can be described independently. One has

$$f^{\rm app}(r,t) \approx \Lambda^2 \bar{\tau} j_{st} \frac{r_0^{\rm app} - 1}{\Lambda r_0^{\rm app} - 1} \exp(-e^{\Lambda\rho}), \tag{57}$$

with

$$r_0^{\rm app} \simeq 1 + (r-1)e^{r-t-1}. \tag{58}$$

The position of the front is given by the asymptote of Eq. (48)

$$r^f \sim t - \ln\frac{t}{\lambda} + \lambda + 1, \quad t \gg 1, \tag{59}$$

so that $\rho = r - r^f$ is an elementary function of r,t, and so is the entire approximation given by Eq. (57). The latter improves the accuracy of the general Eq. (45) at not too large times. For $t \to \infty$, the value of $r_0^{\rm app}$ tends to r_0 in Eq. (34) with $c(\lambda)=\lambda$, and approximation (57) becomes identical to Eq. (45), illustrated in Fig. 3.

3. Long pulse ($\lambda \gg 1$)

Once the pulse is not expected to be shallow, an elementary approximation for r_0 cannot be used, and Eq. (56), which contains the Lambert **W** function, should be involved. Otherwise, the distribution has a similar shape

$$F(\rho) = \Lambda^2 \frac{r_0 - 1}{\Lambda r_0 - 1} \exp(-e^{\Lambda\rho}). \tag{60}$$

This approximation is shown in Fig. 3 and it does provide a good accuracy for λ exceeding several units. Note that the

shape of the front at ρ close to zero is insensitive to the pulse duration.

For a sufficiently long pulse the bulk of the distribution $F(\rho)$ will approach a constant value Λ [which is also the limit of $\nu(\lambda)$ in the general Eq. (38)]. It is convenient to define the width of the distribution as the large absolute value of ρ with $F(\rho)=\Lambda/e$, since $F(0)$-the "front"-has approximately the same magnitude. At $\rho\to-\infty$ one can replace the double-exponential in Eq. (60) by 1, and use $r_0\sim 1+\lambda\exp(\rho+\lambda)$. This gives the width

$$w \simeq \lambda - \ln\frac{\Lambda-1}{\Lambda\lambda(e-1)}, \tag{61}$$

which in the leading approximation is just the length of the tail of the initial distribution, λ, as defined in Fig. 1.

Due to the flatness of the distribution, its maximum is not well pronounced. Nevertheless the location is found to be

$$\rho_{\max} \simeq -\frac{1}{\Lambda}\ln\frac{\Lambda^2(\lambda+1)^2}{\Lambda-1}. \tag{62}$$

This is much smaller than the width, implying a strong asymmetry, with the maximum shifted from the midpoint toward the front. The maximum value is given by

$$F(\rho_{\max}) \simeq \Lambda\left(1-\frac{\Lambda-1}{\Lambda\lambda}\right), \tag{63}$$

which is close to Λ for $\lambda\gg 1$.

Moments of the distribution are given by Eq. (31), which can be represented by

$$M_k = \int_1^{\lambda+1}\frac{dr_0}{\tau^-\dot{r}_0^-}\rho^k + \int_{-\infty}^{0} d\rho\frac{\tau^+\dot{r}_0^+}{\tau^-\dot{r}_0^-}\rho^k(e^{-e^{-x}}-1) + \int_0^{\infty} d\rho\frac{\tau^+\dot{r}_0^+}{\tau^-\dot{r}_0^-}\rho^k e^{-e^{-x}}. \tag{64}$$

The first integral can be easily evaluated since $\rho(r_0)$ is an elementary function, and this integral diverges for $\lambda\to\infty$. The second and third integrals give finite contributions, and are dominated by small $x\simeq-\Lambda\rho$, with $\tau^+\dot{r}_0^+/\tau^-\dot{r}_0^-\simeq\Lambda$. In this manner one obtains $M_0=X-\gamma$, in accord with Eq. (11), and

$$\bar{\rho}=M_1/M_0 \simeq -\frac{\lambda}{2}-\frac{1}{2\Lambda}\ln\lambda-\frac{1}{2\Lambda}\ln\frac{\Lambda}{\Lambda-1}-1+(1-\gamma/2)/\Lambda. \tag{65}$$

The leading term being half of the width, as expected for a near-rectangular box. It is worth reminding, however, that even for λ of several tens deviations from the rectangular shape are appreciable, and the logarithmic corrections are important.

4. Short pulse

The parameter α in Eq. (43) is given by Eqs. (19) and (41). Furthermore, ζ is now just the distance from the maximum, $r-r^{\max}(t)$ with

$$r^{\max}(t) \sim t - \ln t + 1 - \ln(\alpha\mu), \quad \mu=\Lambda^2/(\Lambda-1). \tag{66}$$

The variable ζ also can be used as an argument of the distribution for longer pulse durations, as in Fig. 4. The universal shape emerges for a sufficiently short pulse, $t^n/\tau^- \lesssim 1$, which corresponds to $\alpha\gtrsim 12$ for the parameters considered. λ in this case is negative and has a formal meaning since the initial distribution has no tail.

For large α, with only a tiny fraction of nuclei surviving the growth, numerical accuracy of the maximum $e^{-(\alpha+1)}/\alpha$ is not expected to be too high since the starting double-exponential expression is asymptotic, and can approach the limit of its applicability. Otherwise, comparison with exact numerics[12] reveals that the ζ-dependent shape is accurate and is indeed practically independent of the pulse duration, as long as it remains short.

V. TURNBULL–FISHER MODEL

The discrete analog of Eqs. (1) and (3) is written for the distribution $f_n(t)=f(r,t)dr/dn$, with $n\propto r^3$:

$$df_n/dt = j_n - j_{n+1}, \quad j_n=\beta_{n-1}f_{n-1}-\alpha_n f_n. \tag{67}$$

Boundary conditions are taken as $f_1=1$ and $f_n=0$ for $n=n_{\max}+1$. Kinetic coefficients α_n and β_n are linked by detailed balance $\alpha_n=\beta_{n-1}\exp[(\Phi_n-\Phi_{n-1})/kT]$, with the specific selection $\beta_n=n^{2/3}\exp[(\Phi_n-\Phi_{n+1})/2kT]$ corresponding to a dimensionless version of the TF model[6,7,18,31] (while $\beta_n\propto n^{2/3}$ is the standard BD case—see Appendix B).

Compared with the ZF case, the TF model has a different deterministic growth rate[31]

$$\dot{r}^{\mathrm{TF}}(r) = \frac{2r_*}{a\tau}\sinh\left[\frac{a}{2}\left(1-\frac{r_*}{r}\right)\right]. \tag{68}$$

Here $a=2\Phi_*/(n_*kT)$ plays the role of a "discreteness parameter"[32]—the continuous ZF description emerges for $a\ll 1$. The functional form of Eq. (68) is valid for both the nucleation and the growth stages, albeit with different a, τ, and r_*.

Unlike the ZF model where the growth integral $\int dr/\dot{r}$ evaluates to an elementary function, the TF counterpart $\int dr/\dot{r}^{\mathrm{TF}}$ does not. This makes the latter model analytically more involved. In particular, the expression for the incubation time $t_i^{\mathrm{TF}}(r)$ is not elementary, and the length of the initial tail of the distribution, λ cannot be related to the nucleation parameters even through a special function. Next, Eq. (22)or (28), which relate the nascent size r_0, respectively, to r and t or to ρ, in a general case will have to be solved numerically. All this increases the value of the parametric representation of the general solution. Otherwise, no essential differences from the ZF case are expected, and the latter often can serve as an initial approximation with further corrections obtained iteratively.

If the two models are matched to have identical r_* and τ, one can introduce the dimensionless difference of the inverse rates[33]

$$\delta(r) \equiv |1/(\tau\dot{r}^{\mathrm{TF}})| - |1/(1-1/r)|, \tag{69}$$

which should be specified for the nucleation $(-)$ and for the growth $(+)$ stages, respectively, and which allows to express the results for the TF model as corrections to elementary ZF

expressions. In particular, the incubation time is given by

$$t_i^{\mathrm{TF}}(r) = t_i(r) + \tau^- \int_0^r \delta^-(r')dr', \tag{70}$$

[and for non-negligible lower boundary, which is often the case,[6] zero on the integration limit should be replaced by $r_{\min}/r_*$, with a similar modification of $t_i(r)$ in Eq. (18)]. For moderate values of λ the size-dependent part of the correction is small due to exceptional closeness of $\dot{r}$ and $\dot{r}^{\mathrm{TF}}$ in the vicinity of r_*. The correction in Eq. (70) is then just an a-dependent constant, approximately -0.25,[10] for the parameters considered. The initial position of the front is then determined by the same Eq. (47) with $X^{\mathrm{TF}} \approx X + 0.25$.

Similarly, when describing growth one has

$$\rho = \int_{r_0^f}^{r_0} \frac{dr}{\tau^+ \dot{r}^+} = r_0 - r_0^f + \ln\frac{r_0 - 1}{r_0^f - 1} - \int_{r_0^f}^{r_0} \delta^+(r')dr'. \tag{71}$$

Since the integration involves only the supercritical region with moderate arguments of the sinh-function in $\dot{r}^{\mathrm{TF}}$, the reciprocal of the latter can be expanded in powers of a^+ using the Bernoulli numbers,[33] which leads to

$$\begin{aligned}\int_{r_0^f}^{r_0} \delta^+(r')dr' \simeq{}& \frac{(a^+)^2}{24}\left[r_0 - r_0^f - \ln\frac{r_0}{r_0^f}\right] \\ &- \frac{7(a^+)^4}{1920}\left[\frac{1}{3}(r_0 - r_0^f) + \frac{1}{r_0^f} - \frac{1}{r_0}\right. \\ &\left. + \frac{1}{6}\left(\frac{1}{r_0^2} - \frac{1}{(r_0^f)^2}\right) + \ln\frac{r_0^f}{r_0}\right] + \cdots\end{aligned} \tag{72}$$

Equations (71) and (72) determine ρ, and together with the general Eq. (29) [with $\dot{r}_0$ replaced by $\dot{r}_0^{\mathrm{TF}}$] provide a parametric representation of the asymptotic distribution.

In view of the practical importance, the long pulse approximation for the asymptotic shape will be given explicitly

$$\begin{aligned}F_0(r_0) \simeq{}& \Lambda\frac{a^-}{a^+}\frac{\sinh[a^+/2(1 - 1/r_0)]}{\sinh[a^-/2(1 - 1/\Lambda r_0)]} \\ &\times\exp\{-\exp[\nu_0(r_0 - r_0^f)]\},\end{aligned} \tag{73}$$

with

$$\nu_0 = \Lambda a^-/(2\sinh[a^-/2]). \tag{74}$$

Note that the above is an elementary function, which can be helpful, e.g., when evaluating the maximum, the width, etc., similarly to the ZF case.

Results of comparison with exact numerics, which is described in Appendix A, are shown in Fig. 6 for several long pulses. Although accuracy of the analytical expressions is somewhat less impressive than in the ZF case,[12] they correctly reflect the flat-top structure of the distribution, with the pulse duration affecting the width but not the maximum or the shape of the front.

In contrast, for short pulses the length of the pulse dramatically affect the maximum, but has a minor effect on the width, as in Fig. 7. In the extreme limit of an ultra short

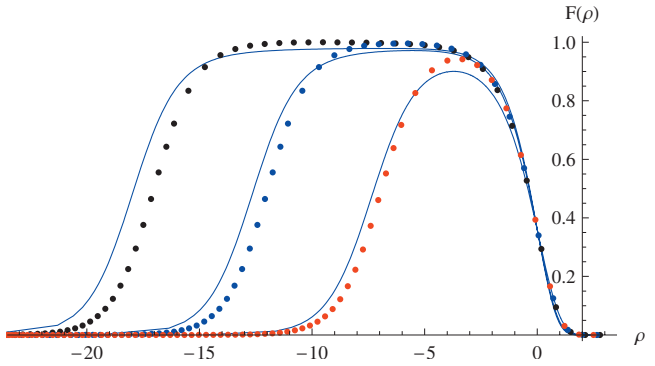

FIG. 6. Distributions after long nucleation pulses with (from right to left) $t^n = 20$, 30 and 40 for the TF nucleation model. Symbols—exact numerics, lines—the large-t^n approximation, Eq. (73) with r_0 replaced by ρ from Eq. (71). Distributions are reduced by $\tau^- j_{st}$; the proximity of the maxima to 1 is coincidental. [The full expression, Eq. (29) not shown in this figure, gives a somewhat better agreement for $t^n = 20$, and is virtually indistinguishable at $t^n = 30$ and 40.]

pulse with the number of particles $N \ll \tau^- j_{st}$, the width of the distribution is not affected by the nucleation conditions, and it follows the universal curve, as in Fig. 4.

Parameter ρ in Eq. (27) is related to physical size r by

$$\rho = \frac{a^+}{2\sinh(a^+/2)}(r - r^f(t)). \tag{75}$$

Due to faster growth the physical distribution slightly broadens compared with the ZF case and, unlike the ZF situation there is no closed analytical expressions for the position of the front r^f at arbitrary time. For $t \to \infty$

$$r^f = \frac{2\sinh(a/2)}{a}t - \frac{a}{2}\coth\frac{a}{2}\ln t + O(1), \quad a = a^+. \tag{76}$$

A similar correction factor appears in the parameter ζ, which describes short-pulse distributions

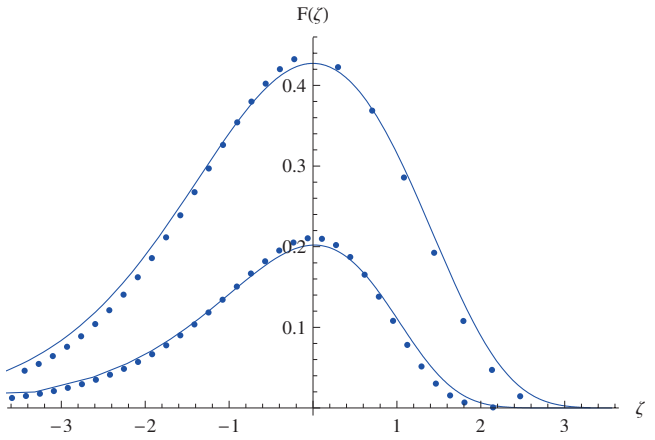

FIG. 7. Distributions after a nucleation pulse of intermediate durations of $t^n = 10$ (upper) and $t^n = 5$ (lower, multiplied by 10). Symbols—numerics (similar to Fig. 6), lines—full asymptotic approximation, Eq. (29), with r_0 replaced by ζ in accord with Eq. (42).

$$\zeta(r) = \frac{a^+}{2\sinh(a^+/2)}(r - r^{\max}(t)), \tag{77}$$

and $r^{\max}(t)$ follows a dependence similar to the one in Eq. (76). Both the maximum and the front accelerate compared with the ZF case.

VI. DISCUSSION

For interface-limited nucleation and growth, a monotonicly decaying distribution of nuclei (as in Fig. 1) is established by the end of the nucleation stage of a pulse. In the vicinity of the nucleation critical size r_*^- this distribution is characterized by very large, near-singular values, and at larger sizes by a tail of dimensionless length λ. An abrupt increase in the critical size to r_*^+ has no immediate effect on this distribution, and the point $r=r_*^+$ at first is in no way remarkable. During subsequent growth, however, the distribution will undergo dramatic changes. First of all, the small-size "singularity" will vanish after a short decay time t_d. Next, the distribution at $r=r_*$ will exponentially decay with time, separating the decay and growth regions of sizes, and leading to a formation of a maximum in the latter. After a sufficiently long growth, an asymptotic shape of the distribution will be established. Typical transformations of the shape for a pulse of intermediate duration are shown in Fig. 5.

In view of the richness of the above transformation picture, the general analytical expression for the distribution $f(r,t)$, with t being the *growth* time, looks remarkably compact, as in Eq. (24) [the nucleation time t^n determines the flux $j(r,0^-)$ via Eq. (8)]. However, additional effort is required to evaluate the "nascent size" r_0 which will grow to size r at time t. For the growth rate associated with the ZF nucleation model, $r_0(r,t)$ can be evaluated in terms of a special function, known as the Lambert **W** function, which leads to a closed formula for the distribution, valid for arbitrary time. For other models, such as the original discrete model due to BD or its modification due to TF, $r_0(r,t)$ has to be evaluated numerically. No significant qualitative differences from the ZF case are expected, but if the nucleation parameters for the models are matched, the TF distribution will be somewhat broader due to faster growth of large particles, while the small-size singularity will disappear earlier due to faster decay. In the BD model the decay is still faster, but growth is slower compared with the ZF case, which should lead to a somewhat narrower, but again qualitatively similar distribution.

After a sufficiently long growth the distribution will approach an asymptotic shape, as in Fig. 5. This shape is characterized by an exponential and double-exponential cutoffs at small and large sizes, respectively, but otherwise is a nontrivial function of two dimensionless parameters, λ and $\Lambda = r_*^+/r_*^-$. A general parametric representation by Eqs. (28) and (29) is the most convenient way to visualize the result.

In the extremes of long and short nucleation pulses, respectively, the asymptotic distribution resembles either an asymmetric trapezoid (e.g., Figures 3 and 6) or an asymmetric bell shape (Figs. 4 and 7). In such cases the pulse duration will have no effect on either the maximum of the distribution (long pulse), or on its width in case of a short pulse.

For practical applications it could be useful to identify situations when the entire shape of the distribution is described in terms of elementary functions. Those include the aforementioned short pulse described by Eqs. (42) and (43), and a longer but "shallow" pulse with additional requirement that increase in the critical size is minor, i.e., Λ is close to 1—see Fig. 3.

A few notes on the possibility to neglect interactions between nuclei, which was mentioned in the Introduction, and which limits the time t. If the flux is normalized per monomer of the matrix [with $j_{st} \sim (1/\tau^-)\exp(-\Phi_*/kT)$] one expects $(t/\tau^+)^3 n_* N \ll 1$, with N being the number of nuclei; this condition will be more relaxed in case of direct impingement if the new phase is much denser than the metastable one. For large $\Phi_* \gg kT$ and, especially for a short pulse with $N \ll \tau^- j_{st}$, the restrictions on t are extremely weak, and there will be plenty of time for the establishment of the described asymptotic shapes, which require a mere nonexponential $t/\tau^+ \gg 1$. More stringent conditions are necessary when considering the *maximum* time t, which can be encountered in an experiment. The upper bound for the ratio t/τ^+ can be estimated as 10^3–10^4—the dimensionless growth time required to bring particles from subnano to micron sizes. The condition of negligible interaction of nuclei formed in a long pulse with $N \sim j_{st} t^n$ (and with $n_* \sim 10^2$) then requires $\Phi_*/kT \gtrsim 32 + \ln(t^n/\tau^-)$. Based on analysis of available experimental data on transient nucleation in lithium disilicate, barriers in excess of $35kT$ are expected,[34] and similar analysis for several other mainstream glasses gives comparable values.[35] Thus, the above requirement is satisfied at least for moderate pulses with $t^n/\tau^- \lesssim 20$. For longer pulses (or lower barriers) interactions of either the Kolmogorov–Avrami or the Lifshits–Slyozov type are expected to broaden the distribution and round-off its flat top, and to destroy the conserved feature of the number of nuclei N, turning it into a decaying function of the growth time t.

Another potential limitation of the treatment comes from continuing nucleation, i.e., non-negligible j_{st}^+ during the growth stage. Due to very long growth times, such nucleation will result in a near-steady-state "secondary" distribution with a constant value $j_{st}^+/\dot{r}^+ \sim \exp(-\Phi_*^+/kT^+)$ (here the + and the − superscripts will be re-introduced explicitly to distinguish the growth and the nucleation stages). This should be small compared with the maximum of the primary distribution. For a long pulse, where the maximum is t^n-independent, one obtains

$$\exp\left(\frac{\Phi_*^+}{kT^+} - \frac{\Phi_*^-}{kT^-}\right) \gg 1.$$

Note that this condition does not include $\tau^{\pm}$, which otherwise can significantly re-distribute the nucleation rates (as a rule, τ^+ is much smaller than τ^- in crystallization experiments). The above condition is usually satisfied, but for a short pulse it should be refined since the primary maximum rapidly drops with decreasing t^n. For an ultra short pulse the maximum is roughly estimated as $\exp(X - e^{-X} - \Phi_*^-/kT^-)$, with a negative X given by Eq. (19). In that case one has

$$\frac{\Phi_*^+}{kT^+} \gtrsim \frac{\Phi_*^-}{kT^-} + e^{-X} - X,$$

which in practice limits from below the length of a detectable nucleation pulse.

Conditions of negligible nucleation on the growth stage will change if one considers the moments, which are usually detected in experiments, rather than the distribution itself. This is due to different structures of the primary distribution, which is narrow in terms of r, and the secondary one, which is broad. In order to distinguish the primary distribution from a δ-function, one needs at least the first correction in Eq. (30). For a given k, determined by specific experimental technique, the above correction should be compared with the corresponding moment of the secondary distribution, which can be estimated as $1/(k+1)(r^f)^{k+1} j_{st}^+ / \dot{r}_\infty^+$. With $r^f \sim r_*^+ t/\tau^+$ for the ZF growth rate, and with $r_*^+ \sim r_*^-$, one thus obtains for a long pulse

$$\left(\frac{t}{\tau^+}\right)^2 \exp\left(-\frac{\Phi_*^+}{kT^+}\right) \ll \frac{k(k+1)}{2}\left(\frac{t^n}{\tau^-}\right)^2 \exp\left(-\frac{\Phi_*^-}{kT^-}\right).$$

For selected nucleation and growth times the above condition establishes a lower boundary on Φ_*^+/kT^+. For example, for the already discussed $t^n/\tau^- \lesssim 10^1$ and $t/\tau^+ \lesssim 10^4$ (and with $k \sim 1$) one requires $\Phi_*^+/kT^+ - \Phi_*^-/kT^- \gtrsim 14$. This is satisfied for parameters used in the numerical scheme with a relatively large $\Phi_*^+/kT^+ \approx 58$ (and with $\Phi_*^-/kT^- \approx 37$), but generally speaking care should be taken here since direct experimental data for the barrier on the growth stage are often unavailable. In practice, if the possibility to neglect secondary nucleation is unclear, one could use a "superposition principle," evaluating the corresponding moment at $t^n = 0$, and subtracting this value from similar measurements at nonzero nucleation times.

VII. CONCLUSION

Based on a singular perturbation solution of the BD nucleation equations, the distribution function of nuclei over sizes following a nucleation pulse has been obtained analytically. This distribution is asymmetric, with a much sharper cutoff at large sizes, and it ranges in shape from a near-rectangular box of a fixed height, to a bell-shape of a fixed width in the limits of very long and very short pulses, respectively. Results are shown to be accurate numerically, and can be useful for experiments based on the technique of a nucleation pulse, such as the two-step annealing crystallization studies.

APPENDIX A: NUMERICS

In order to mimic realistic conditions of two-step annealing in lithium disilicate[1,2] nucleation at $730^0 K$ and growth at $840^0 K$ were considered with parameters consistent with earlier Ref. 10, and close to those used by other groups.[6,7,31] Specifically, for the nucleation stage $n_* \simeq 18.2$, $\Phi_*/kT \simeq 36.9$, $\tau \simeq 1.94$, $a \simeq 4.06$, and for the growth stage $n_* \simeq 40.0$, $\Phi_*/kT \simeq 58.2$, $\tau \simeq 3.53$, $a \simeq 2.91$. (Note that time units are dimensionless; in order to convert to physical units one needs to match the TF rate $\dot{r}_\infty$ to experimental growth rate u,[36]). The upper boundary $n_{\max}$ was taken as 105 and insensitivity to the selection was verified.

The general approach to solve the BD equations with TF coefficients was described by Kelton co-workers.[6,31] In the present study a matrix representation similar to the one in Ref. 37 was used, with the forward update scheme implemented in *Mathematica 6*. The flux at a large size $n^{\rm up}$, close to $n_{\max}$, was treated as "nucleation rate."

Specifically, when solving Eq. (67) distribution f_n was represented as a d-dimensional vector $\vec{f} = (f_2, \cdots, f_{d+1})$ with $d = n_{\max} - 1$. The update was written in terms of a propagator $\mathcal{P}$ as

$$\vec{f}(t+\epsilon) = \mathcal{P} \cdot \vec{f}(t) + \epsilon \beta_1 \vec{e}, \quad \mathcal{P} = \hat{I} + \epsilon \hat{M}. \tag{A1}$$

Here $\hat{I}$ is a $d \times d$ identity matrix, $\vec{e} = (1,0,0,\ldots,0)$, a d-dimensional unit vector, and $\hat{M}$ is a sparse, tridiagonal matrix with nonzero elements

$$M_{i,i} = -(\alpha_{i+1} + \beta_{i+1}), \quad M_{i,i+1} = \alpha_{i+1}, \quad M_{i+1,i} = \beta_{i+1}. \tag{A2}$$

The step ϵ was selected as $(10^{-3} - 10^{-2})\tau^-$ to ensure stability of the scheme. The update scheme was applied on both the nucleation and the growth stages, with the distribution established by the end of the former serving as initial condition for the latter. Nucleated particles were further grown deterministically (see below), and a seamless transition between stochastic and deterministic distributions between $n^{\rm up}$ and $n_{\max}$ served as indicator of consistency of numerics.

Distribution of deterministically growing nuclei $f(r,t)$ was approximated by a histogram with a variable number of bins. Each bin represented some size r, which increased in time in accord with the deterministic growth law as $\dot{r}^{\rm TF}\Delta t$. At each growth step $\Delta t \sim (10^1 - 10^2)\epsilon$ a new bin was added at the smallest growth size, corresponding to $n = n^{\rm up}$, with the content of the bin given by

$$\sum_{m=1}^{\Delta t/\epsilon} j_n(t + m\epsilon).$$

For clarity, only selected points representing distributions are shown in the figures, and no distinction is made between the deterministic (growth) and the stochastic (nucleation) domains.

In the present work the ZF was solved numerically on the nucleation stage in order to check the accuracy of initial conditions for growth, as in Fig. 1; numerics for the growth stage is reported in Ref. 12. One notes that the ZF model emerges as a limit of the TF one for a large critical number n_*, if the barrier Φ_* is fixed. To achieve this without changes to the algorithm, the free energy difference between phases was multiplied by a small $\delta \simeq 1/8$, while the interfacial tension was multiplied by $\delta^{2/3}$ to preserve the barrier but increase the value of $n_* \propto 1/\delta$, thus minimizing the discreteness effects. In order to engulf the large $n_*^+ \simeq 320$ in this limit an $n_{\max} = 600$ was used, which determined the longest computational time, about $1h$ for a single nucleation-grow run in extreme cases. In this sense, the ZF model is computationally

much more involved than the TF one when describing nucleation. The ZF model, however, allows a closed-form analytical description of growth. Indeed, a size r_1 observed at time t_1 will acquire a larger value r after a selected time t, with r given by

$$r = 1 + \mathbf{W}[(r_1 - 1)\exp(r_1 - 1 + t - t_1)].$$

This allows one to start with a histogram $f(r_1, t_1)$ obtained numerically after a modest growth time t_1, and to "anneal" this distribution analytically by using arbitrarily large t and

$$f(r,t) = f(r_1,t_1)\frac{\dot{r}_1}{\dot{r}}.$$

Results obtained using this technique are reported in Ref. 12. In contrast, the TF model requires a numerical annealing during a much longer time t_1 in order to achieve a typical $r_1 \gg 1$ and to observe the asymptotic regime described above.

APPENDIX B: BECKER–DÖRING MODEL

In the standard BD case the gain coefficient β_n in Eq. (67) is proportional to $n^{2/3}$. This leads to a known growth rate

$$\dot{r}^{\mathrm{BD}} = \frac{r_*}{a\tau}\left\{1 - \exp\left[-a\left(1 - \frac{r_*}{r}\right)\right]\right\}, \tag{B1}$$

with the discreteness parameter a having the same meaning as before, and the ZF growth rate emerging in the limit $a \to 0$.

The general analysis is similar to the one for the TF model in Sec. V. One can introduce δ, the difference of $1/\tau\dot{r}^{\mathrm{BD}}$ from the inverse of the ZF rate, and express the BD expectations for $t_i(r)$ and ρ as corrections to elementary ZF expressions. Assuming all three models have identical τ and j_{st}, the following differences are anticipated.

Since the BD model has the fastest decay and the slowest growth, the incubation time $t_i^{\mathrm{BD}}(r)$ will be smaller than the ZF counterpart $t_i(r)$ for small r and larger for large r, respectively (see a similar analysis for the time-lag,[32] which differs by a constant $\gamma\tau$.) This is in contrast with the TF case with $t_i^{\mathrm{TF}}(r) < t_i(r)$ for *any* r. Thus, as follows from Eq. (10), while the TF model will predict a larger number of nuclei N compared with the ZF case for similar nucleation times t^n, the BD model will give either more or less particles than ZF for smaller or larger Λ, respectively, with the crossover Λ^* determined by a. Similar conclusions apply to the length of the tail of the nucleation distribution, as in Fig. 1.

During the growth stage, the BD model will lead to the fastest disappearance of the nucleation singularity due to faster decay. General expressions for the asymptotic shapes will remain valid, but connection with physical size r is now given by

$$\rho \sim \frac{a^+}{1 - \exp(-a^+)}(r - r^f), \tag{B2}$$

and a similar factor appears in $\zeta \propto (r - r^{\max})$. The front (or the maximum) will increase at the slowest rate, and asymptotically its position is given by

$$r^f = \frac{1 - e^{-a}}{a}t - \frac{a}{e^a - 1}\ln t + O(1), \quad a = a^+. \tag{B3}$$

If the number of particles N is matched for every one of the three models (implying a slightly different t^n in each case), the TF distribution will be the widest and the BD one the narrowest in r-variables.

[1] P. James, Phys. Chem. Glasses **15**, 95 (1974).
[2] J. Deubener, R. Brükner, and M. Sternizke, J. Non-Cryst. Solids **163**, 1 (1993).
[3] Y. T. Shen, T. H. Kim, A. K. Gangopadhyay, and K. F. Kelton, Phys. Rev. Lett. **102**, 057801 (2009).
[4] C. Spinella, S. Lombardo, and F. Priolo, J. Appl. Phys. **84**, 5383 (1998).
[5] G. Nicotra, R. A. Puglisi, S. Lombardo, C. Spinella, M. Vulpio, G. Ammendola, M. Bileci, and C. Gerardi, J. Appl. Phys. **95**, 2049 (2004).
[6] K. F. Kelton, A. L. Greer, and C. V. Thompson, J. Chem. Phys. **79**, 6261 (1983).
[7] L. Granasy and P. James, J. Chem. Phys. **113**, 9810 (2000).
[8] M. Davis, Glass Sci. Technol. (Offenbach, Ger.) **73**, 171 (2000); J. Am. Ceram. Soc. **84**, 492 (2001).
[9] V. A. Shneidman, Sov. Phys. Tech. Phys. **33**, 1338 (1988).
[10] V. A. Shneidman, J. Chem. Phys. **127**, 041102 (2007).
[11] U. Gasser, E. R. Weeks, A. Schofield, P. N. Pusey, and D. A. Weitz, Science **292**, 258 (2001).
[12] V. A. Shneidman, Phys. Rev. Lett. **101**, 205702 (2008).
[13] R. S. Sidin, R. Hagmeijer, and U. Sachs, Phys. Fluids **21**, 073303 (2009).
[14] D. van Putten and V. Kalikmanov, J. Chem. Phys. **130**, 164508 (2009); V. Holten and M. E. H. van Dongen, *ibid.* **130**, 014102 (2009).
[15] J. Wolk, R. Strey, C. H. Heath, and B. E. Wyslouzil, J. Chem. Phys. **117**, 4954 (2002).
[16] Ya. B. Zeldovich, Acta Physicochim. URSS **18**, 1 (1943).
[17] J. Frenkel, *Kinetic Theory of Liquids* (Oxford University, Oxford, 1946).
[18] D. Turnbull and J. C. Fisher, J. Chem. Phys. **17**, 71 (1949).
[19] L. Farkas, Z. Phys. Chem. **25**, 236 (1927).
[20] R. Becker and W. Döring, Ann. Phys. **416**, 719 (1935).
[21] A. N. Kolmogorov, Bull. Acad. Sci. USSR (Sci. Mater. Nat.) **3**, 3551 (1937).
[22] M. Avrami, J. Chem. Phys. **7**, 1103 (1939).
[23] I. M. Lifshits and V. V. Slyozov, Zh. Eksp. Teor. Fiz **35**, 479 (1958) [Sov. Phys. JETP **8**, 331 (1959)].
[24] C. Wagner, Z. Elektrochem. **65**, 581 (1961).
[25] V. A. Shneidman, Phys. Rev. Lett. **95**, 115701 (2005).
[26] V. A. Shneidman, Sov. Phys. Tech. Phys. **32**, 76 (1987).
[27] V. A. Shneidman, Phys. Lett. A **143**, 275 (1990).
[28] V. A. Shneidman, J. Chem. Phys. **115**, 8141 (2001).
[29] M. Abramowitz and I. Stegun, *Handbook of Mathematical Functions* (Dover, New York, 1972).
[30] V. A. Shneidman, J. Chem. Phys. **119**, 12487 (2003).
[31] K. F. Kelton and A. L. Greer, J. Non-Cryst. Solids **79**, 295 (1986).
[32] V.A. Shneidman and M. C. Weinberg, J. Chem. Phys. **97**, 3629 (1992).
[33] V. A. Shneidman and E. V. Goldstein, J. Non-Cryst. Solids **351**, 1512 (2005).
[34] V. A. Shneidman and M. C. Weinberg, Ceram. Trans. **30**, 275 (1993).
[35] J. Deubener, private communication (1994).
[36] V. A. Shneidman and D. R. Uhlmann, J. Chem. Phys. **109**, 186 (1998).
[37] V. A. Shneidman and G. M. Nita, Phys. Rev. Lett. **97**, 065703 (2006).